Latin American Journal of Solids and Structures
www.lajss.org

Sound Transmission across Orthotropic Cylindrical Shells Using Third-order Shear Deformation Theory

Abstract

The objective of this paper is representation of an analytical solution to calculate transmission loss (TL) of an arbitrarily thick cylindrically orthotropic shell, immersed in a fluid medium with a uniform external airflow and contains internal fluids. The shell is assumed to be infinitely long and is excited by an oblique plane wave. The displacements are expanded as cubic functions of the thickness coordinate to present an analytical solution based on Third-order Shear Deformation Theory (TSDT). Equations of motion of the shell are then obtained using virtual work method. By solving shell vibration as well as acoustic wave equations simultaneously, the exact solution for TL is obtained. Predictions with the presented models are compared with those of previous models (CST and FSDT) for thin shells. Similar results are achieved as the effects of shear and rotation on TL are not noticeable in a thin shell. However, the model introduced here exhibits more accurate results for thick shells where the shear and rotation effects become more significant in lower R/h ratios. Additionally, the effects of related parameters on TL such as material and geometrical properties are discussed.

Keywords

Orthotropic shells, Transmission loss, Third order shear deformation theory, Acoustic.

M. H. Shojaeefard 1 [a]
R. Talebitooti 2 [b,c]
R. Ahmadi 3 [d]
M. R.Gheibi 4 [e]

[a] Prof., Sch. of Mech. Eng., Iran Univ. of Sci. and Tech., Iran, mhshf@iust.ac.ir
[b] Asst. Prof., Sch. of Mech. Eng., Iran Univ. of Sci. and Tech., Iran, rtalebi@iust.ac.ir.
[c] Automotive Simulation & Optimal Design Research Lab., Sch. of Auto. Eng., Iran Univ. of Sci. and Tech., Tehran, Iran.
[d] PhD. Stu., Sch. of Auto. Eng., Iran Univ. of Sci. and Tech., Iran, rahmadi@auto.iust.ac.ir
[e] PhD. Stu., Sch. of Auto. Eng., Iran Univ. of Sci. and Tech., Iran,m_gheybi@auto.iust.ac.ir

Nomenclature

c_3, c_1	Speed of sound in external and cavity medium	TL	Transmission Loss
E	Module of elasticity	(u_1, u_2, u_3)	Displacements of a point on the plane $\eta_3 = 0$
f_r	Ring frequency	V	Velocity of the external flow
f_c	Critical frequency	W^I	Incident power flow per unit length
G	Shear stiffness	W^T	Transmitted power flow per unit length
h	Shell wall thickness	α	Incident angle
H_n^1	Cylindrical Henkel functions of the first kind of integer order n	$\alpha_{\max}, \alpha_{\min}$	Critical angles of incidence
H_n^2	Cylindrical Henkel functions of the second kind of integer order n	δK	Virtual kinetic energy
I_n	Mass inertia	δU	Virtual strain energy
J_n	Cylindrical Bessel function of the first kind of order n	δV	Virtual potential energy
k	Wave number	ε_n	Neumann factor
k_r, k_z	Wave numbers in η_3 and η_1 direction	(η_1, η_2, η_3)	Displacements of the shell in the radial, circumferential and axial directions
M_1	Mach number	υ	Poisson's ratio
n	Circumferential mode number	ω	Angular frequency
P_0	Amplitude of the incident wave	ρ	Mass density of shell per unit mid-surface area
P_1^I	Acoustic pressures of the incident wave	ρ_3, ρ_1	Density of external and internal medium
P_1^R	Acoustic pressures of the reflected wave	σ_{ij}	Stress components
P_3^T	Acoustic pressure of the transmitted wave	τ_{ij}	Strain (shear strain) components
q_i	Transverse load on the surface of the shell	$\overline{\tau}$	Average power transmission coefficient
Q_{ij}	Orthotropic reduced stiffness coefficients	ϕ_i	Rotations of transverse normal on plane $\eta_3 = 0$
R	Radii of cylinder	∇	Laplacian operator
t	Time	Ω_0	Mid-surface of the shell

1 INTRODUCTION

Acoustic transmission is investigated in this study through an arbitrarily thick orthotropic cylinder of infinite length, which is excited by a diffuse field. This issue has been addressed in the literatures to a large extent. Several attempts have performed significant studies on isotropic, orthotropic and laminated fiber-reinforced composite shells. Smith (1957) developed a theoretical study in isotropic cylindrical shells taking into account inward-traveling wave as an only parameter. TL was then introduced by the same author as the ratio of absorbed power to incident power per unit length. White (1966) analyzed sound transmission into finite cylindrical shells and obtained two important characteristics, namely ring frequency and coincidence frequency, with maximum values of the obtained TL. Koval (1976 and 1979) utilized displacement field of Nelson et al. (1958) to show mathematical models for estimation of the TL of oblique plane sound waves through an orthotropic infinite shell. The effects of membrane and bending were considered as well, though transverse shearing and rotational inertia were not taken into account. The effect of orthotropic behavior on TL was parametrically studied for the shell's elastic properties along circumferential and axial directions. The main feature of his contribution was considering external airflow, external plane wave with an incident angle and internal pressure of the cylindrical shell. Transmission of airborne noise was studied by this solution through isotropic and orthotropic fuselage under flight conditions using impedance method. An analytical model was suggested by Koval (1980) for predicting TL of laminated composite infinite cylindrical shells excited by an oblique plane wave. Transverse shearing and rotational inertia were not considered in this research work. Blaise et al. (1991) extended Koval's (1979) work and followed an orthotropic shell excited by an oblique plane sound wave with two independent incident angles for calculation of the diffuse field transmission coefficient. They compared the numerical results with Koval's results and found some numerical errors in his work. In their study, they used a Donnell–Mushtari's displacements field for orthotropic cylinders ignoring transverse shearing and rotational inertia. Diffuse field transmission coefficient was calculated based on two independent incident angles. Moreover, they extended definition of the ring and critical frequencies to an infinite orthotropic shell excited by a plane wave. Furthermore, a model was developed for acoustic transmission of the oblique incidence of multi-layered cylindrical shells (Blaise et al., 1992). Finally, the same authors presented a new model taking into account 3D displacement fields in thickness for the acoustic transmission through an orthotropic multi-layered infinite cylindrical shell (Blaise et al., 1994). Tang et al. (1996) studied sound transmission through infinite cylindrical sandwich shells illuminated an oblique plane wave with two different incident angles. They presumed same Blaise's assumptions for incident angles and acoustic media. The effects of external airflow and pressure difference between inside and outside shell surfaces were considered in their study for different fluids in both sides of the shell. They utilized first order shell theory for thick shells to calculate the TL.

Lee and Kim (2002 and 2003) calculated the sound transmission in cylindrical shells using analytical and experimental models. The inside cavity was assumed to be anechoic, whereas the incident wave was a plane wave. The shell vibration motions were described by the Love's equation. They considered all three displacement fields and both transverse and in-plane equations to depict the shell motion. They applied a convergence algorithm to calculate TL. Eventually, they could present a comparison between analytical and experimental models. Ghinet et al. (2006) developed

two models for calculating diffuse field transmission into composite laminate and sandwich composite infinite cylinders. They considered membrane, bending, transverse shearing as well as rotational inertia effects and orthotropic ply angle of the layers in both models.

Classical shell theory (CST) was utilized in most of the above citations to model the shell vibration. However, it cannot be used for thick shells and even thin shells when the number of circumferential waves increases as the result of neglecting shear deformation and rotary inertia effects in CST. Implementation of CST for thick and relatively thick shells can cause significant errors in such cases. An exact solution was found by Daneshjou et al. (2007, 2008 and 2009) more recently in a series form based on CST and first order shear deformation theory (FSDT). They considered all three displacements of the shell for orthotropic and laminated composite cylindrical shells. They also showed that considering the effects of shear and rotation in FSDT for thin shells leads to reduction of TL in high frequency range in comparison with CST. Just recently, Daneshjou et al. (2010) proposed an improved model for sound transmission through relatively thick FGM cylindrical shells based on third order shear deformation theory (TSDT). In addition, they have shown that for relatively thick FGM shells where the shear and rotation effects become more significant in lower R/h ratio, TSDT presents more accurate results.

The existing literature lacks a comprehensive work on sound transmission of thick orthotropic cylindrical shells. In order to modify previous studies, noting that the best presented model in literature can not include the proper modeling for thick shells due to its assumptions on the straightness and normality of transverse normal during deformation. Therefore, in this paper it has been tried to use third order shear deformation theory (TSDT) which relaxes these assumptions by expanding the displacements as cubic functions of the thickness coordinate. Thus, this paper presents a novel and accurate modeling of the acoustic transmission of a thick-wall orthotropic cylindrical shell with subsonic external flow based on TSDT. Then, the obtained results are compared with those available in the literature. The comparison reveals a good agreement. This paper also intends to quantify the effects of orthotropic cylindrical shell characteristics on TL. At last, the numerical results are used to address the effects of geometrical properties and material properties.

2 STATEMENT OF THE PROBLEM

Figure 1 depicts an orthotropic cylindrical shell of infinite length, radius, R, wall thickness, h and mass density of shell per unit mid-surface area, ρ, which is irradiated to an oblique plane wave with the incident angle of α from outside. A uniform external airflow at velocity V in the exterior fluid medium impinges on the shell. Moreover, ρ_i and c_i with subscripts 1 and 3 are used respectively to introduce external and internal density and also the speed of acoustic media. Also, the interior side of the shell is assumed to be anechoic, which means that only inward-traveling wave exists. As shown in the Figure 1, (η_1, η_2, η_3) denote the orthogonal curvilinear coordinate system where the η_1 is coincident with the axis of cylindrical shell, while η_2 and η_3 are circumferential and thickness directions, respectively.

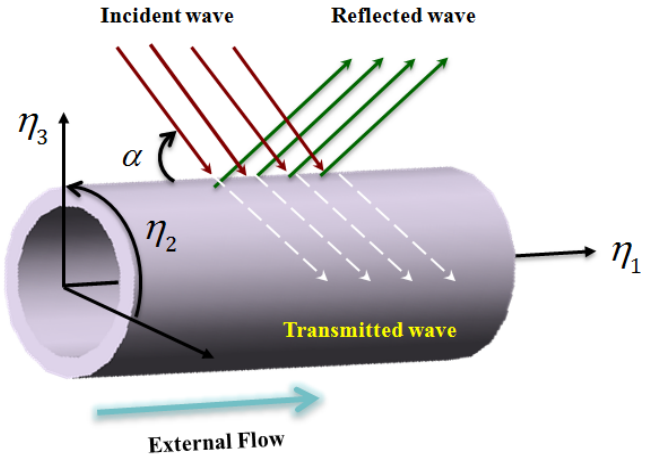

Figure 1: Schematic diagram of the cylindrical shell

3 THEORITICAL FORMULATIONS

Particular assumptions are considered in developing a thick shell theory as follows (Reddy, 2003):
(1) The transverse normal is inextensible (i.e. $\varepsilon_{33} = 0$).
(2) There is no reason for straightness and normality of a transverse normal during deformation.
(3) The transverse normal stress is negligible in order that the plane stress assumption cannot be considered.
These assumptions will be used in formulation of the problem.

3.1 Kinematic relations

For the cylindrical shells, the strain-displacement relation can be presented as (Qatu, 2004):

$$\varepsilon_{11} = \frac{\partial U_1}{\partial \eta_1} \quad ; \quad \varepsilon_{22} = \frac{1}{R\left(1+\frac{\eta_3}{R}\right)}\left[\frac{\partial U_2}{\partial \eta_2} + U_3\right] \quad ; \quad \varepsilon_{33} = \frac{\partial U_3}{\partial \eta_3}$$

$$\varepsilon_{12} = \frac{1}{R\left(1+\frac{\eta_3}{R}\right)}\frac{\partial}{\partial \eta_2}U_1 + R\left(1+\frac{\eta_3}{R}\right)\frac{\partial}{\partial \eta_1}\left(\frac{U_2}{R\left(1+\frac{\eta_3}{R}\right)}\right) \tag{1}$$

$$\varepsilon_{13} = \frac{\partial U_1}{\partial \eta_3} + \frac{\partial U_3}{\partial \eta_1} \quad ; \quad \varepsilon_{23} = R\left(1+\frac{\eta_3}{R}\right)\frac{\partial}{\partial \eta_3}\left(\frac{U_2}{R\left(1+\frac{\eta_3}{R}\right)}\right) + \frac{1}{R\left(1+\frac{\eta_3}{R}\right)}\frac{\partial U_3}{\partial \eta_2}$$

where R is the radii of cylinder and (U_1, U_2, U_3) represent the shell displacements along (η_1, η_2, η_3) coordinates. It should be mentioned the only assumption made here is the small displacements. No other assumptions are considered in this formulation.

3.2 Stress – strain relations

The stress-strain relations for an orthotropic cylindrical shell can be presented by the Hook's law as (Chakrabartiet al., 2013):

$$\begin{Bmatrix} \sigma_{11} \\ \sigma_{22} \\ \sigma_{12} \\ \sigma_{13} \\ \sigma_{23} \end{Bmatrix} = \begin{bmatrix} Q_{11} & Q_{12} & 0 & 0 & 0 \\ Q_{21} & Q_{22} & 0 & 0 & 0 \\ 0 & 0 & Q_{66} & 0 & 0 \\ 0 & 0 & 0 & Q_{55} & 0 \\ 0 & 0 & 0 & 0 & Q_{44} \end{bmatrix} \begin{Bmatrix} \varepsilon_{11} \\ \varepsilon_{22} \\ \varepsilon_{12} \\ \varepsilon_{13} \\ \varepsilon_{23} \end{Bmatrix} \tag{2}$$

where σ_{ij} and ε_{ij} denote stress and strain components in the orthotropic layer and Q_{ij}, denotes the in-plane-stress reduced stiffness constants that are defined in terms of material properties of the orthotropic ply, which can be defined as:

$$Q_{11} = \frac{E_1}{1-\nu_{12}\nu_{21}} \quad ; \quad Q_{12} = \frac{\nu_{12}E_2}{1-\nu_{12}\nu_{21}} \quad ; \quad Q_{22} = \frac{E_2}{1-\nu_{12}\nu_{21}}$$
$$Q_{44} = G_{23} \quad ; \quad Q_{55} = G_{13} \quad ; \quad Q_{66} = G_{12} \tag{3}$$

where E_{11} and E_{22} are respectively the module of elasticity in η_1 and η_2 directions, while G_{23}, G_{13} and G_{12} are the modules of rigidity and υ_{12} and υ_{21} represent the Poisson's ratios.

Relaxing the straightness and normality of a transverse normal during deformation, the displacement field for third-order shear deformation theory represented as (Lee and Reddy, 2004, Chakrabarti, 2013):

$$U_1(\eta_1,\eta_2,\eta_3,t) = u_1(\eta_1,\eta_2,t) + \eta_3\phi_1(\eta_1,\eta_2,t) - C_1{\eta_3}^3(\phi_1 + \frac{\partial u_3}{\partial \eta_1})$$
$$U_2(\eta_1,\eta_2,\eta_3,t) = u_2(\eta_1,\eta_2,t) + \eta_3\phi_2(\eta_1,\eta_2,t) - C_1{\eta_3}^3(-\frac{u_2}{R} + \phi_2 + \frac{\partial u_3}{R\partial \eta_2}) \tag{4}$$
$$U_3(\eta_1,\eta_2,\eta_3,t) = u_3(\eta_1,\eta_2,t) \quad ; \quad \phi_1(\eta_1,\eta_2,t) = \frac{\partial U_1}{\partial \eta_3} \quad ; \quad \phi_2(\eta_1,\eta_2,t) = \frac{\partial U_2}{\partial \eta_3}$$

where (u_1, u_2, u_3) are the displacements of a point on plane η_3, (ϕ_1, ϕ_2) are the rotations of transverse normal. The constant C_1 is given by $C_1 = 4h^2 / 3$.

As a result, substitution of Eq. (4) into the strain–displacement relations of shell, Eq. (1), strains would be written as:

$$\begin{Bmatrix}\varepsilon_{11}\\ \varepsilon_{22}\\ w_1\\ w_2\end{Bmatrix}=\begin{Bmatrix}\varepsilon_{11}^{(0)}\\ \varepsilon_{22}^{(0)}\\ w_1^{(0)}\\ w_2^{(0)}\end{Bmatrix}+\eta_3\begin{Bmatrix}\varepsilon_{11}^{(1)}\\ \varepsilon_{22}^{(1)}\\ w_1^{(1)}\\ w_2^{(1)}\end{Bmatrix}+{\eta_3}^3\begin{Bmatrix}\varepsilon_{11}^{(3)}\\ \varepsilon_{22}^{(3)}\\ w_1^{(3)}\\ w_2^{(3)}\end{Bmatrix}$$
$$\begin{Bmatrix}\varepsilon_{13}\\ \varepsilon_{23}\end{Bmatrix}=\begin{Bmatrix}\varepsilon_{13}^{(0)}\\ \varepsilon_{23}^{(0)}\end{Bmatrix}+{\eta_3}^2\begin{Bmatrix}\varepsilon_{13}^{(2)}\\ \varepsilon_{23}^{(2)}\end{Bmatrix}+{\eta_3}^3\begin{Bmatrix}\varepsilon_{13}^{(3)}\\ \varepsilon_{23}^{(3)}\end{Bmatrix} \tag{5}$$

where

$$\begin{Bmatrix}\varepsilon_{11}^{(0)}\\ w_1^{(0)}\end{Bmatrix}=\begin{Bmatrix}\dfrac{\partial u_1}{\partial\eta_1}\\ \dfrac{\partial u_2}{\partial\eta_1}\end{Bmatrix}\quad;\quad\begin{Bmatrix}\varepsilon_{11}^{(1)}\\ w_1^{(1)}\end{Bmatrix}=\begin{Bmatrix}\dfrac{\partial\phi_1}{\partial\eta_1}\\ \dfrac{\partial\phi_2}{\partial\eta_1}\end{Bmatrix}$$
$$\begin{Bmatrix}\varepsilon_{11}^{(3)}\\ w_1^{(3)}\end{Bmatrix}=-\frac{C_1}{R}\begin{Bmatrix}R(\dfrac{\partial\phi_1}{\partial\eta_1}+\dfrac{\partial^2u_3}{\partial{\eta_1}^2})\\ -\dfrac{\partial u_2}{\partial\eta_1}+R\dfrac{\partial\phi_2}{\partial\eta_1}+\dfrac{\partial^2u_3}{\partial\eta_1\partial\eta_2}\end{Bmatrix}$$
$$\begin{Bmatrix}\varepsilon_{22}^{(0)}\\ w_2^{(0)}\end{Bmatrix}=C_2\begin{Bmatrix}\dfrac{1}{R}(\dfrac{\partial u_2}{\partial\eta_2}+u_3)\\ \dfrac{1}{R}\dfrac{\partial u_1}{\partial\eta_2}\end{Bmatrix}\quad;\quad\begin{Bmatrix}\varepsilon_{22}^{(1)}\\ w_2^{(1)}\end{Bmatrix}=C_2\begin{Bmatrix}\dfrac{1}{R}\dfrac{\partial\phi_2}{\partial\eta_2}\\ \dfrac{\partial\phi_2}{\partial\eta_1}+\dfrac{1}{R}\dfrac{\partial\phi_1}{\partial\eta_2}\end{Bmatrix} \tag{6}$$
$$\begin{Bmatrix}\varepsilon_{22}^{(3)}\\ w_2^{(3)}\end{Bmatrix}=-\frac{C_1C_2}{R}\begin{Bmatrix}\dfrac{\partial\phi_2}{\partial\eta_2}+\dfrac{\partial^2u_3}{R\partial{\eta_2}^2}-\dfrac{\partial u_2}{R\partial\eta_2}\\ \dfrac{\partial\phi_1}{\partial\eta_2}+\dfrac{\partial^2u_3}{\partial\eta_1\partial\eta_2}\end{Bmatrix}$$
$$\begin{Bmatrix}\varepsilon_{13}^{(0)}\\ \varepsilon_{23}^{(0)}\end{Bmatrix}=\begin{Bmatrix}\phi_1+\dfrac{\partial u_3}{\partial\eta_1}\\ C_2(\phi_2+\dfrac{1}{R}\dfrac{\partial u_3}{\partial\eta_2}-\dfrac{u_2}{R})\end{Bmatrix}\quad;\quad\begin{Bmatrix}\varepsilon_{13}^{(2)}\\ \varepsilon_{23}^{(2)}\end{Bmatrix}=-3C_1\begin{Bmatrix}\varepsilon_{13}^{(0)}\\ \varepsilon_{23}^{(0)}\end{Bmatrix}\quad;\quad\begin{Bmatrix}\varepsilon_{13}^{(3)}\\ \varepsilon_{23}^{(3)}\end{Bmatrix}=-\frac{2C_1}{R}\begin{Bmatrix}\varepsilon_{13}^{(0)}\\ \varepsilon_{23}^{(0)}\end{Bmatrix}$$

where $C_2=\dfrac{1}{1+(\eta_3\ /\ R)}$.

3.3 Stress resultant

The force and moment resultants are achieved by integrating the stresses over the shell thickness. The normal and shear force resultants are:

$$\begin{Bmatrix} N_{11} \\ N_{12} \\ Q_{13} \end{Bmatrix} = \int_{-\frac{h}{2}}^{\frac{h}{2}} \left(1 + \frac{\eta_3}{R}\right) \begin{Bmatrix} \sigma_{11} \\ \sigma_{12} \\ \sigma_{13} \end{Bmatrix} d\eta_3 \quad ; \quad \begin{Bmatrix} N_{22} \\ N_{21} \\ Q_{23} \end{Bmatrix} = \int_{-\frac{h}{2}}^{\frac{h}{2}} \begin{Bmatrix} \sigma_{22} \\ \sigma_{12} \\ \sigma_{23} \end{Bmatrix} d\eta_3 \tag{7}$$

The bending and twisting moment resultants and higher order shear resultant terms are:

$$\begin{Bmatrix} M_{11} \\ P_{11} \\ M_{12} \\ P_{12} \\ R_{13} \\ P_{13} \end{Bmatrix} = \int_{-\frac{h}{2}}^{\frac{h}{2}} \left(1 + \frac{\eta_3}{R_1}\right) \begin{Bmatrix} \eta_3\sigma_{11} \\ \eta_3{}^3\sigma_{11} \\ \eta_3\sigma_{12} \\ \eta_3{}^3\sigma_{12} \\ \eta_3{}^2\sigma_{13} \\ \eta_3{}^3\sigma_{13} \end{Bmatrix} d\eta_3 \quad ; \quad \begin{Bmatrix} M_{22} \\ P_{22} \\ M_{21} \\ P_{21} \\ R_{23} \\ P_{23} \end{Bmatrix} = \int_{-\frac{h}{2}}^{\frac{h}{2}} \begin{Bmatrix} \eta_3\sigma_{22} \\ \eta_3{}^3\sigma_{22} \\ \eta_3\sigma_{12} \\ \eta_3{}^3\sigma_{12} \\ \eta_3{}^2\sigma_{23} \\ \eta_3{}^3\sigma_{23} \end{Bmatrix} d\eta_3 \tag{8}$$

The dimensions of force and moment resultants are force per unit length and moment per unit length, respectively. Also, by substitution of Eqs. (5) and (6) into the stress-strain relations in Eq. (2) and expressing resultants into Eqs. (7) and (8) can be written:

$$\{F\} = \begin{bmatrix} [S_{11}] & [S_{12}] & [S_{13}] \\ [S_{21}] & [S_{22}] & [S_{23}] \\ [S_{31}] & [S_{32}] & [S_{33}] \end{bmatrix} \{Y\}$$

$$\{F\}^T = \{N_{11}, M_{11}, P_{11}, N_{12}, M_{12}, P_{12}, Q_{13}, R_{13}, P_{13}\}$$

$$[S_{11}] = \begin{bmatrix} A_{11} & B_{11} & E_{11} & A_{12} & B_{12} & E_{12} \\ B_{11} & D_{11} & F_{11} & B_{12} & D_{12} & F_{12} \\ E_{11} & F_{11} & H_{11} & E_{12} & F_{12} & H_{12} \end{bmatrix}$$

$$[S_{22}] = \begin{bmatrix} A'_{66} & B'_{66} & E'_{66} & A_{66} & B_{66} & E_{66} \\ B'_{66} & D'_{66} & F'_{66} & B_{66} & D_{66} & F_{66} \\ E'_{66} & F'_{66} & H'_{66} & E_{66} & F_{66} & H_{66} \end{bmatrix} \tag{9}$$

$$[S_{33}] = \begin{bmatrix} A_{55} & D_{55} & E_{55} \\ D_{55} & F_{55} & G_{55} \\ E_{55} & G_{55} & H_{55} \end{bmatrix}$$

$$[S_{12}] = [S_{21}] = [S_{31}] = [S_{32}] = [0]_{3\times 6}$$

$$[S_{13}] = [S_{23}] = [0]_{3\times 3}$$

$$\{Y\}^T = \left\{\varepsilon_{11}^{(0)}, \varepsilon_{11}^{(1)}, \varepsilon_{11}^{(3)}, \varepsilon_{22}^{(0)}, \varepsilon_{22}^{(1)}, \varepsilon_{22}^{(3)}, w_1^{(0)}, w_1^{(1)}, w_1^{(3)}, w_2^{(0)}, w_2^{(1)}, w_2^{(3)}, \varepsilon_{13}^{(0)}, \varepsilon_{13}^{(2)}, \varepsilon_{13}^{(3)}\right\}$$

and

$$\left\{\overline{F}\right\} = \begin{bmatrix} \left[\overline{S}_{11}\right] & \left[\overline{S}_{12}\right] & \left[\overline{S}_{13}\right] \\ \left[\overline{S}_{21}\right] & \left[\overline{S}_{22}\right] & \left[\overline{S}_{23}\right] \\ \left[\overline{S}_{31}\right] & \left[\overline{S}_{32}\right] & \left[\overline{S}_{33}\right] \end{bmatrix} \left\{\overline{Y}\right\}$$

$$\left\{\overline{F}\right\}^T = \left\{N_{22}, M_{22}, P_{22}, N_{21}, M_{21}, P_{21}, Q_{23}, R_{23}, P_{23}\right\}$$

$$\left[\overline{S}_{11}\right] = \begin{bmatrix} A_{21} & B_{21} & E_{21} & A_{22} & B_{22} & E_{22} \\ B_{21} & D_{21} & F_{21} & B_{22} & D_{22} & F_{22} \\ E_{21} & F_{21} & H_{21} & E_{22} & F_{22} & H_{22} \end{bmatrix}$$

$$\left[\overline{S}_{22}\right] = \begin{bmatrix} A_{66} & B_{66} & E_{66} & A''_{66} & B''_{66} & E''_{66} \\ B_{66} & D_{66} & F_{66} & B''_{66} & D''_{66} & F''_{66} \\ E_{66} & F_{66} & H_{66} & E''_{66} & F''_{66} & H''_{66} \end{bmatrix} \tag{10}$$

$$\left[\overline{S}_{33}\right] = \begin{bmatrix} A_{44} & D_{44} & E_{44} \\ D_{44} & F_{44} & G_{44} \\ E_{44} & G_{44} & H_{44} \end{bmatrix}$$

$$\left[\overline{S}_{12}\right] = \left[\overline{S}_{21}\right] = \left[\overline{S}_{31}\right] = \left[\overline{S}_{32}\right] = \left[0\right]_{3\times 6}$$

$$\left[\overline{S}_{13}\right] = \left[\overline{S}_{23}\right] = \left[0\right]_{3\times 3}$$

$$\left\{\overline{Y}\right\}^T = \left\{\varepsilon_{11}^{(0)}, \varepsilon_{11}^{(1)}, \varepsilon_{11}^{(3)}, \varepsilon_{22}^{(0)}, \varepsilon_{22}^{(1)}, \varepsilon_{22}^{(3)}, w_1^{(0)}, w_1^{(1)}, w_1^{(3)}, w_2^{(0)}, w_2^{(1)}, w_2^{(3)}, \varepsilon_{23}^{(0)}, \varepsilon_{23}^{(2)}, \varepsilon_{23}^{(3)}\right\}$$

where

$$\begin{Bmatrix} A_{11}, B_{11}, D_{11}, E_{11}, F_{11}, G_{11}, H_{11} \\ A_{55}, B_{55}, D_{55}, E_{55}, F_{55}, G_{55}, H_{55} \\ A'_{66}, B'_{66}, D'_{66}, E'_{66}, F'_{66}, G'_{66}, H'_{66} \end{Bmatrix} = \int_{-\frac{h}{2}}^{\frac{h}{2}} \begin{Bmatrix} Q_{11} \\ Q_{55} \\ Q_{66} \end{Bmatrix} (1 + \frac{\eta_3}{R}) \left\{1, \eta_3, {\eta_3}^2, {\eta_3}^3, {\eta_3}^4, {\eta_3}^5, {\eta_3}^6\right\} d\eta_3$$

$$\begin{Bmatrix} A_{22}, B_{22}, D_{22}, E_{22}, F_{22}, G_{22}, H_{22} \\ A_{44}, B_{44}, D_{44}, E_{44}, F_{44}, G_{44}, H_{44} \\ A''_{66}, B''_{66}, D''_{66}, E''_{66}, F''_{66}, G''_{66}, H''_{66} \end{Bmatrix} = \int_{-\frac{h}{2}}^{\frac{h}{2}} \begin{Bmatrix} Q_{22} \\ Q_{44} \\ Q_{66} \end{Bmatrix} \left(\frac{1}{1 + \frac{\eta_3}{R}}\right) \left\{1, \eta_3, {\eta_3}^2, {\eta_3}^3, {\eta_3}^4, {\eta_3}^5, {\eta_3}^6\right\} d\eta_3 \tag{11}$$

$$\begin{Bmatrix} A_{12}, B_{12}, D_{12}, E_{12}, F_{12}, G_{12}, H_{12} \\ A_{21}, B_{21}, D_{21}, E_{21}, F_{21}, G_{21}, H_{21} \\ A_{66}, B_{66}, D_{66}, E_{66}, F_{66}, G_{66}, H_{66} \end{Bmatrix} = \int_{-\frac{h}{2}}^{\frac{h}{2}} \begin{Bmatrix} Q_{12} \\ Q_{21} \\ Q_{66} \end{Bmatrix} \left\{1, \eta_3, {\eta_3}^2, {\eta_3}^3, {\eta_3}^4, {\eta_3}^5, {\eta_3}^6\right\} d\eta_3$$

3.4 Equations of motion

Now, the displacement field, Eq. (4), can be utilized to derive the governing equations of the third-order shear deformation theory of orthotropic shells by means of Hamilton's principle. It can be obtained as:

$$\int_0^T \delta L dt = \int_0^T [\delta K + \delta V - \delta U] dt = 0 \tag{12}$$

In which δK, δU and δV are the virtual kinetic energy, the virtual strain energy and the virtual potential energy due to the applied loads, respectively and are given by:

$$\delta K = \int_V \rho \left(\dot{U}_1 \delta \dot{U}_1 + \dot{U}_2 \delta \dot{U}_2 + \dot{U}_3 \delta \dot{U}_3 \right) dV$$

$$\begin{aligned} &= \int_{\Omega_0} \int_{-\frac{h}{2}}^{\frac{h}{2}} \rho \ [(\dot{u}_1 + \eta_3 \dot{\phi}_1 - C_1 {\eta_3}^3 (\dot{\phi}_1 + \frac{\partial \dot{u}_3}{\partial \eta_1}))(\delta \dot{u}_1 + \eta_3 \delta \dot{\phi}_1 - C_1 {\eta_3}^3 (\delta \dot{\phi}_1 + \frac{\partial \delta \dot{u}_3}{\partial \eta_1})) + \\ &(\dot{u}_2 + \eta_3 \dot{\phi}_2 - C_1 {\eta_3}^3 (-\frac{u_2}{R} + \dot{\phi}_2 + \frac{\partial \dot{u}_3}{R \partial \eta_2}))(\delta \dot{u}_2 + \eta_3 \delta \dot{\phi}_2 - C_1 {\eta_3}^3 (-\frac{\delta u_2}{R} + \\ &\delta \dot{\phi}_2 + \frac{\partial \delta \dot{u}_3}{R \partial \eta_2})) + \dot{u}_3 \boldsymbol{\delta} \dot{u}_3] \times \left[R \left(1 + \frac{\eta_3}{R} \right) d\eta_3 d\eta_1 d\eta_2 \right] \end{aligned} \tag{13}$$

$$\delta U = \int_V \sigma_{ij} \, \delta \varepsilon_{ij} \, dV = \int_{\Omega_0} \int_{-\frac{h}{2}}^{\frac{h}{2}} \sigma_{ij} \, \delta \varepsilon_{ij}$$

$$\begin{aligned} &= \int_{\Omega_0} \int_{-\frac{h}{2}}^{\frac{h}{2}} [\sigma_{11} (\delta \varepsilon_{11}^{(0)} + \eta_3 \delta \varepsilon_{11}^{(1)} + {\eta_3}^3 \delta \varepsilon_{11}^{(3)}) + \sigma_{22} \left(\frac{1}{1 + \frac{\eta_3}{R}} \right) (\delta \varepsilon_{22}^{(0)} + \eta_3 \delta \varepsilon_{22}^{(1)} + {\eta_3}^3 \delta \varepsilon_{22}^{(3)}) + \\ &\sigma_{12} ((\delta w_1^{(0)} + \eta_3 \delta w_1^{(1)} + {\eta_3}^3 \delta w_1^{(3)}) + \left(\frac{1}{1 + \frac{\eta_3}{R}} \right) \left(\delta w_2^{(0)} + \eta_3 \delta w_2^{(1)} + {\eta_3}^3 \delta w_2^{(3)} \right)) + \\ &\sigma_{13} (\delta \varepsilon_{13}^{(0)} + {\eta_3}^2 \delta \varepsilon_{13}^{(2)} + {\eta_3}^3 \delta \varepsilon_{13}^{(3)}) + \\ &\sigma_{23} \left(\frac{1}{1 + \frac{\eta_3}{R}} \right) (\delta \varepsilon_{23}^{(0)} + {\eta_3}^2 \delta \varepsilon_{23}^{(2)} + {\eta_3}^3 \delta \varepsilon_{23}^{(3)})] \times \left[R \left(1 + \frac{\eta_3}{R_2} \right) d\eta_3 d\eta_1 d\eta_2 \right] \end{aligned} \tag{14}$$

Also, using Eqs. (7) and (8), the virtual strain energy equation can be re-written as below:

$$\delta U = \int_{\Omega_0}[(N_{11}\delta\varepsilon_{11}^{(0)} + M_{11}\delta\varepsilon_{11}^{(1)} + P_{11}\delta\varepsilon_{11}^{(3)}) + \left(N_{22}\delta\varepsilon_{22}^{(0)} + M_{22}\delta\varepsilon_{22}^{(1)} + P_{22}\delta\varepsilon_{22}^{(3)}\right) + \left(N_{12}\delta w_1^{(0)} + M_{12}\delta w_1^{(1)} + P_{12}\delta w_1^{(3)}\right) + \left(N_{21}\delta w_2^{(0)} + M_{21}\delta w_2^{(1)} + P_{21}\delta w_2^{(3)}\right) + \left(Q_{13}\delta\varepsilon_{13}^{(0)} + R_{13}\delta\varepsilon_{13}^{(2)} + P_{13}\delta\varepsilon_{13}^{(3)}\right) + \left(Q_{23}\delta\varepsilon_{23}^{(0)} + R_{23}\delta\varepsilon_{23}^{(2)} + P_{23}\delta\varepsilon_{23}^{(3)}\right) \times R d\eta_1 d\eta_2 \tag{15}$$

and virtual potential energy would be equal to:

$$\delta V = \int_{\Omega_0}\int_{-\frac{h}{2}}^{\frac{h}{2}} \left(q_1\delta u_1 + q_2\delta u_2 + q_3\delta u_3 + q_4\delta\phi_1 + q_5\delta\phi_2\right) \times \left[R\left(1+\frac{h}{2R}\right)d\eta_1 d\eta_2\right] d\eta_3 \tag{16}$$

where Ω_0 denotes mid-surface of the shell.

By substitution of δK, δU and δV from Eqs. (13) to (16) into Eq. (12) and then considering that the virtual generalized displacements are zero at $t = 0$ and $t = T$, the equations of motion for cylindrical shell are obtained as follows:

$$-\left(-R\frac{\partial N_{11}}{\partial\eta_1} - \frac{\partial N_{21}}{\partial\eta_2}\right) - \left(\bar{K}\frac{\partial^2 u_1}{\partial t^2} + \bar{J}\frac{\partial^2\phi_1}{\partial t^2} + C_1 R K_4\frac{\partial\ddot{u}_3}{\partial\eta_1}\right) + R\left(1+\frac{h}{2R}\right)q_1 = 0 \tag{17}$$

$$-\left(-\frac{\partial N_{22}}{\partial\eta_2} - \frac{C_1}{R}\frac{\partial P_{22}}{\partial\eta_2} - R\frac{\partial N_{12}}{\partial\eta_1} - C_1\frac{\partial P_{12}}{\partial\eta_1} - Q_{23} + 3C_1 R_{23} + \frac{2C_1}{R}P_{23}\right) - \left(\bar{W}\frac{\partial^2 u_2}{\partial t^2} + \bar{G}\frac{\partial^2\phi_1}{\partial t^2} - C_1 W_4\frac{\partial\ddot{u}_3}{\partial\eta_2}\right) + R\left(1+\frac{h}{2R}\right)q_2 = 0 \tag{18}$$

$$C_1 R\frac{\partial^2 P_{11}}{\partial{\eta_1}^2} - N_{22} + \frac{C_1}{R}\frac{\partial^2 P_{22}}{\partial{\eta_2}^2} + C_1\left(\frac{\partial^2 P_{12}}{\partial\eta_1\partial\eta_2} + \frac{\partial^2 P_{21}}{\partial\eta_1\partial\eta_2}\right) + R\frac{\partial Q_{13}}{\partial\eta_1} + \frac{\partial Q_{23}}{\partial\eta_2} - 3C_1\left(R\frac{\partial R_{13}}{\partial\eta_1} + \frac{\partial R_{23}}{\partial\eta_2}\right) - \frac{2C_1}{R}\frac{\partial P_{23}}{\partial\eta_2} - C_1 W_4\frac{\partial\ddot{u}_2}{\partial\eta_2} - C_1 J_5\frac{\partial\ddot{\phi}_2}{\partial\eta_2} - C_1 R K_4\frac{\partial\ddot{u}_1}{\partial\eta_1} - C_1 R J_5\frac{\partial\ddot{\phi}_1}{\partial\eta_1} - R I_1\frac{\partial^2 u_3}{\partial t^2} + {C_1}^2 I_7 R\left(\frac{\partial^2\ddot{u}_3}{\partial{\eta_1}^2} + \frac{1}{R^2}\frac{\partial^2\ddot{u}_3}{\partial{\eta_2}^2}\right) + R\left(1+\frac{h}{2R}\right)q_3 = 0 \tag{19}$$

$$-\left(-R\frac{\partial M_{11}}{\partial\eta_1} + C_1 R\frac{\partial P_{11}}{\partial\eta_1} + C_1\frac{\partial P_{21}}{\partial\eta_2} - \frac{\partial M_{21}}{\partial\eta_2} + R(Q_{13} - 3C_1 R_{13})\right) - \left(\tilde{K}\frac{\partial^2 u_1}{\partial t^2} + \tilde{J}\frac{\partial^2\phi_1}{\partial t^2} - C_1 R J_5\frac{\partial\ddot{u}_3}{\partial\eta_1}\right) + R\left(1+\frac{h}{2R}\right)q_4 = 0 \tag{20}$$

$$-\left(-\frac{\partial M_{22}}{\partial \eta_2}+C_1\frac{\partial P_{22}}{\partial \eta_2}+C_1R\frac{\partial P_{12}}{\partial \eta_1}-R\frac{\partial M_{12}}{\partial \eta_1}+R(Q_{23}-3C_1R_{23})\right)$$
$$-\left(\tilde{W}\frac{\partial^2 u_2}{\partial t^2}+\tilde{J}\frac{\partial^2 \phi_2}{\partial t^2}-C_1J_5\frac{\partial \ddot{u}_3}{\partial \eta_2}\right)+R\left(1+\frac{h}{2R}\right)q_5=0 \tag{21}$$

where q_3 is the transversal load on the shell's surface and I_i is the mass inertias. Hence, Eqs. (22) and (23) would be found as below:

$$\{q\}=[0,0,\left(P_1^I+P_1^R\right)-P_3^T,0,0]^T \tag{22}$$

and

$$I_i=\int_{-\frac{h}{2}}^{\frac{h}{2}}\rho\,\eta_3{}^{i-1}(1+\frac{\eta_3}{R})d\eta_3\ ;\qquad \left(i=1,2,3,4,5,6,7\ \right) \tag{23}$$

The other terms are summarized as follows:

$$W_i=I_i+\left(\frac{C_1}{R}\right)I_{i+3}\ ;\qquad \left(i=1,2,3,4\right)$$
$$K_i=I_i\ ;\qquad \left(i=1,2,3,4\right) \tag{24}$$
$$J_i=I_i-C_1I_{i+2}\ ;\qquad \left(i=1,2,3,4,5\right)$$

and

$$\bar{K}=RK_1\quad ;\quad \bar{J}=RJ_2\quad ;\quad \bar{G}=R\left(J_2+\left(\frac{C_1}{R}\right)J_5\right)\quad ;\quad \bar{W}=R\left(W_1+\left(\frac{C_1}{R}\right)W_4\right)$$
$$\tilde{W}=R\left(W_2-C_1W_4\right)\quad ;\quad \tilde{K}=R\left(K_2-C_1K_4\right)\quad ;\quad \tilde{J}=R\left(J_3-C_1J_5\right) \tag{25}$$

3.5 Wave equations

The harmonic incident plane wave, P_1^I, in cylindrical coordinate (see Figure 1) can be expressed as (Daneshjouet al., 2008):

$$P_1^I\left(\eta_1,\eta_2,\eta_3,t\right)=P_0\sum_{n=0}^{\infty}\epsilon_n\left(-j\right)^n J_n\left(k_{1r}\eta_3\right)\exp\left[j\left(\omega t-k_{1z}\eta_1-n\eta_2\right)\right] \tag{26}$$

where P_0 is the amplitude of the incident wave; J_n represents the Bessel function of the first kind of order n, ω denotes the angular frequency and $j=\sqrt{-1}$. Other undefined parameters are:

$$\epsilon_n=\begin{cases}1 & (n=0)\\ 2 & (n\geq 1)\end{cases};\qquad k_{1z}=k_1\cos(\alpha)\;;\qquad k_{1r}=k_1\sin(\alpha) \tag{27}$$

where k_1 is the wave number in the moving medium that can be written as:

$$k_1=\frac{\omega}{c_1}\left(\frac{1}{1+M_1\sin\left(\alpha\right)}\right) \tag{28}$$

in which $M_1=V\;/\;c_1$ is the Mach number of the external flow.

Moreover, since the traveling wave in the acoustic media and cavity of the shell are driven by the incident traveling wave, the wave numbers in η_3 direction should match throughout the system, therefore:

$$k_{3z}=k_{1z}\;;\qquad k_{3r}=\sqrt{{k_3}^2-{k_{3z}}^2}\;;\qquad k_3=\frac{\omega}{c_3} \tag{29}$$

The wave radiated from the shell to the outside and inside the cavity, respectively is written in the following forms:

$$P_1^R\left(\eta_1,\eta_2,\eta_3,t\right)=\sum_{n=0}^{\infty}P_{1n}^R H_n^2\left(k_{1r}\eta_3\right)\exp\left[j\left(\omega t-k_{1z}\eta_1-n\eta_2\right)\right] \tag{30}$$

$$P_3^T\left(\eta_1,\eta_2,\eta_3,t\right)=\sum_{n=0}^{\infty}P_{3n}^T H_n^1\left(k_{1r}\eta_3\right)\exp\left[j\left(\omega t-k_{1z}\eta_1-n\eta_2\right)\right] \tag{31}$$

where H_n^1 and H_n^2 are the cylindrical Hankel functions of first and second kinds of order n, respectively. In the external space, the pressure $P_1=P_1^I+P_1^R$ satisfies the following wave equation (Daneshjou et al., 2009; Howe, 2000):

$$c_1^2\nabla^2\left(P_1^I+P_1^R\right)-\left(\frac{\partial}{\partial t}+V\;.\nabla\right)^2\left(P_1^I+P_1^R\right)=0 \tag{32}$$

where ∇^2 is the Laplacian operator in the cylindrical coordinate system, P_1^I and P_1^R denote the acoustic pressures of the incident and reflected waves, respectively. The acoustic pressure of the transmitted wave, P_3^T ,in the internal cavity satisfies the acoustic wave equation:

$$c_3^2 \nabla^2 P_3^T - \frac{\partial^2 P_3^T}{\partial t^2} = 0 \tag{33}$$

3.6 Vibro-acoustic boundary conditions

The acceleration of the fluid particle through the acoustic media in the normal direction has to be equal to the normal acceleration of the shell. Based on Helmholtz equations in the internal and external spaces, boundary conditions of the model can be defined as (Daneshjou et al., 2009, Howe, 2000):

$$\frac{\partial\left(P_1^I + P_1^R\right)}{\partial \eta_3} = -\rho_1 \left(\frac{\partial}{\partial t} + V \,.\nabla\right)^2 U_3 \,, \qquad \eta_3 = R \tag{34}$$

$$\frac{\partial P_3^T}{\partial \eta_3} = -\rho_3 \frac{\partial^2 U_3}{\partial t^2} \,, \qquad \eta_3 = R \tag{35}$$

3.7 Vibro-acoustic solution

The displacement and rotation terms of the mid-surface can be written as follows:

$$\begin{Bmatrix} u_1 \\ u_2 \\ u_3 \\ \phi_1 \\ \phi_2 \end{Bmatrix} = \sum_{n=0}^{\infty} \begin{bmatrix} jU_{1n} \\ jU_{2n} \\ U_{3n} \\ j\phi_{1n} \\ j\phi_{2n} \end{bmatrix} \exp\left[j\left(\omega t - k_{1z}\eta_1 - n\eta_2\right)\right] \tag{36}$$

Eventually, by substituting Eqs. (26) to (31) and also Eq. (36) into the shell equations of motion and boundary conditions equations (Eqs. (34) and (35)), the following 7×7 coupled linear systems of equations are obtained in terms of circumferential mode number and frequency. These seven equations involve eight variables including amplitudes of the outgoing and incoming waves in the exterior cavity, transmitted wave in the interior cavity, three displacements and two rotations of the shell structure. These equations are solved simultaneously with considering the pressure amplitude of the incident wave as the independent variable and the other seven unknown variables $U_{1n}, U_{2n}, U_{3n}, \phi_{1n}, \phi_{2n}, P_{1n}^R, P_{3n}^T$ in terms of P_0 .

$$\left[A\right]\left\{X\right\} = \left[B\right] \tag{37}$$

where

$$\left[A\right]=\begin{bmatrix} A_{11} & A_{12} & A_{13} & A_{14} & A_{15} & 0 & 0 \\ A_{21} & A_{22} & A_{23} & A_{24} & A_{25} & 0 & 0 \\ A_{31} & A_{32} & A_{33} & A_{34} & 0 & A_{36} & A_{37} \\ A_{41} & A_{42} & A_{43} & A_{44} & A_{45} & 0 & 0 \\ A_{51} & A_{52} & A_{53} & A_{54} & A_{55} & 0 & 0 \\ 0 & 0 & A_{63} & 0 & 0 & A_{66} & 0 \\ 0 & 0 & A_{73} & 0 & 0 & 0 & A_{77} \end{bmatrix} \tag{38}$$

$$\left\{X\right\}=\left[U_{1n},U_{2n},U_{3n},\phi_{1n},\phi_{2n},P_{1n}^{R},P_{3n}^{T}\right]^{T} \tag{39}$$

$$\left[B\right]=\left[0,0,B_3,0,0,B_6,0\right]^{T} \tag{40}$$

Elements of $\left[A\right]$ and $\left[B\right]$ are given in Appendix.

3.8 Transmission loss

TL can be defined as the ratio of incoming and transmitted sound power per unit length of the cylinder (Lee and Kim, 2003). Hence:

$$TL=10\log_{10}\left(\frac{W^{I}}{W^{T}}\right) \tag{41}$$

where W^{T} is the transmitted power flow per unit length of the shell and can be written by:

$$W^{T}=\frac{1}{2}\mathrm{Re}\left\{\int_{0}^{2\pi}P_{3}^{T}\frac{\partial}{\partial t}(U_{3})^{*}rd\eta_{2}\right\},\qquad r=R \tag{42}$$

where $\mathrm{Re}\{...\}$ and the superscript *, represent the real part and the complex conjugate of the argument, respectively. Calculating the components of P_{3}^{T} and U_{3} from Eq. (37), W^{T} will be equal to:

$$\begin{aligned} W_{n}^{T}&=\frac{1}{2}\mathrm{Re}\left\{P_{3}^{T}H_{n}^{1}\left(k_{3r}r\right).\left(j\omega U_{3n}\right)^{*}\right\}\int_{0}^{2\pi}cos^{2}\left(n\theta\right)Rd\theta\ ,\qquad r=R \\ &=\frac{\pi R}{\epsilon_{n}}\times\mathrm{Re}\left\{P_{3}^{T}H_{n}^{1}\left(k_{3r}r\right).\left(j\omega U_{3n}\right)^{*}\right\} \end{aligned} \tag{43}$$

and the incident power flow per unit length of the shell is:

$$W^I = \frac{\sin(\alpha) P_0^{\,2}}{\rho_1 c_1} R \tag{44}$$

Finally, the TL can be obtained by substituting Eqs. (43) and (44) into Eq. (41):

$$TL = -10\log_{10}\tau(\alpha) = -10\log_{10}\sum_{n=0}^{\infty}\frac{\mathrm{Re}\left\{P_{3n}^{T} H_n^1\left(k_{3r}R\right)\left(j\omega U_3\right)^*\right\}\rho_1 c_1 \pi}{\epsilon_n cos\left(\alpha\right) P_0^{\,2}} \tag{45}$$

In case of a diffuse field excitation, the average power transmission coefficientin the diffuse field is given as (Pierce, 1981):

$$\overline{\tau} = \int_{\alpha_{\min}}^{\alpha_{\max}} \tau(\alpha)\sin(\alpha)\cos(\alpha)\, d\alpha \tag{46}$$

where $\tau(\alpha)$ is the power transmission coefficient calculated for the incident angle, α. Also $\alpha_{\min}$ and $\alpha_{\max}$ are critical angles of incidence. The average TL_{ave} is given as (Lee and Kim, 2003):

$$TL_{ave} = 10\log_{10}\left(\frac{1}{\overline{\tau}}\right) \tag{47}$$

4 CONVERGENCE PROCEDURE

A convergence checking is required in this analysis due to the fact that the solutions are expressed in series form and the use of infinite numbers of modes is unfeasible. Therefore, an iterative procedure in each frequency is constructed, considering the maximum iteration number. Unless that the convergence condition is met, it iterates again. The solution is considered to be convergent at each frequency, when the TLs calculated at two successive calculations are within a pre-set error bound (10^{-8} dB in this work). Figure 2 depicts the concept of this convergence. This algorithm enables the code to consider sufficient terms for the series form solution in calculating the TL.

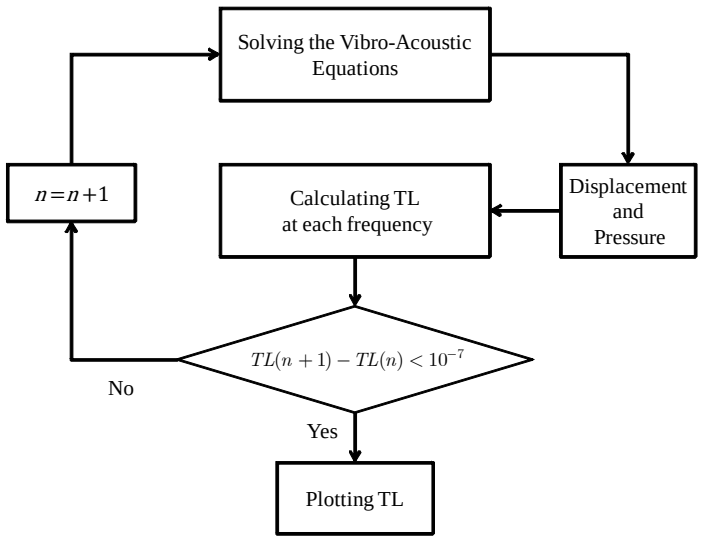

Figure 2: Algorithm for identifying the optimum mode number

Figure 3 shows the convergence of TL curves at 10 kHz for a Glass/Epoxy cylindrical shell whose properties are listed in Table 1 (Daneshjou et al., 2009). As illustrated in Figure 3, by increasing the radius of the shell, the number of modes to achieve a converged solution is increased. As shown in Table 2, increasing the frequency has a direct effect on the convergence and hence more numbers of modes are needed at high frequency. In addition, as the accuracy of the results increase, the number of required modes also increases.

Material	**Shell**					**Cavity**	**Ambient**
	Aluminum	Steel	Graphite/Epoxy	Glass/Epoxy	Boron/Epoxy	Air	Air
$\rho\ (kg\ /\ m^3)$	2760	7750	1600	1900	1600	0.94	0.3795
$E_{11}(GPa)$	72	210	137.9	38.6	206	-	-
$E_{22}(GPa)$	72	210	8.96	8.2	20.6	-	-
$G_{12}(GPa)$	27.7	80.77	7.1	4.2	6.89	-	-
$G_{13}(GPa)$	27.7	80.77	7.1	4.2	6.89	-	-
$G_{23}(GPa)$	27.7	80.77	6.2	3.45	4.1	-	-
υ_{12}	0.3	0.3	0.3	0.26	0.3	-	-
$c\ (m\ /\ s)$	-	-	-	-	-	328.5	296.6
$R\ (m)$	1.5						
$h\ (mm)$	1.5						
$\alpha(^{\circ})$	45						

Table 1: Environmental and Geometrical properties.

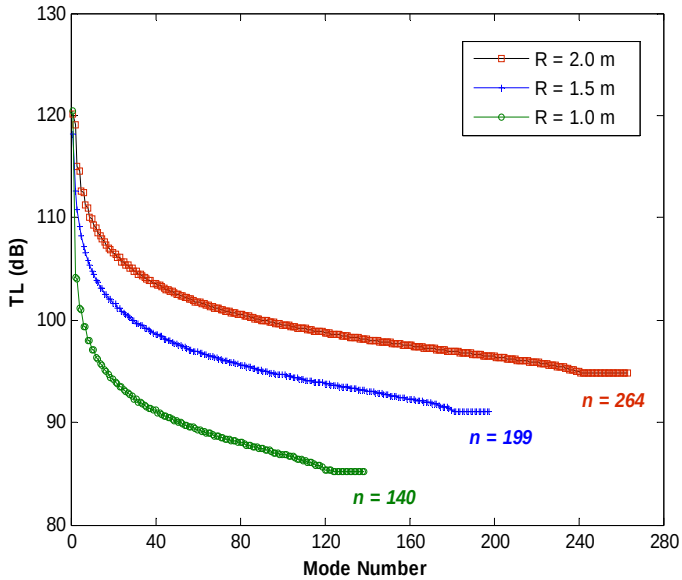

Figure 3: Mode convergence diagram for Glass/Epoxy cylindrical shell at 10 kHz

Error Band (dB)	Radius (m)	Thickness (mm)	Frequency (Hz)	Mode Number
10^{-6}	**1**	10	100	6
			1000	20
			10000	134
	1.5	15	100	6
			1000	28
			10000	193
	2	20	100	7
			1000	32
			10000	253
10^{-8}	**1**	10	100	6
			1000	21
			10000	140
	1.5	15	100	7
			1000	30
			10000	199
	2	20	100	8
			1000	34
			10000	264

Table 2: Effect of radius, thickness and frequency on mode convergence

5 RESULTS AND DISCUSSION

In order to validate the present formulation and the developed code, the results obtained for the shells have been compared with those of the literature. Firstly, the analytical model presented by Lee and Kim (2003) and statistical energy analysis (SEA) are employed to validate the results for the special case of isotropic shell. Then, the model impedance method is utilized using the work presented by Koval (1979) for an orthotropic cylindrical shell.

In Figure 4 the results of TSDT are compared with those of Lee and Kim's (2003) for an isotropic steel shell with characteristics as listed in Table 1. It can be seen that there is a good agreement between the results of two theories in the figure. The little differences are observed due to some numerical errors in calculation of the incident and transmitted powers in Kim's model.

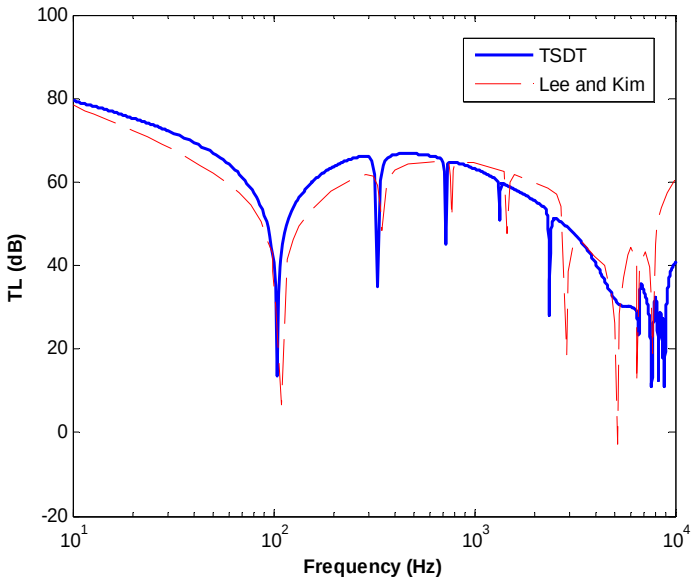

Figure 4: Comparison of present study (TSDT) with Lee and Kim

Figure 5 compares the diffuse field transmission loss (TL_{ave}) obtained from the present model with the numerical results achieved by statistical energy analysis approach using a wave number approach based on the proposed discrete laminate theory. Details of calculations of the required parameters (modal density, damping and coupling loss factor and radiation efficiency) for the SEA calculations are represented by Ghinet (2006) and Yuan (2012).

As illustrated in Figure 5, the predicted TL_{ave} obtained from the present model reveals a good agreement with the SEA simulation, particularly at high-frequency. SEA is based on simulating the vibro-acoustic energy flow between subsystems of the full system. It is very good in the study of sound and vibration transmission through complex structures at high frequencies. However, it is notreliable at low frequencies due to the statistical uncertainties that occur when there are few resonant modes in each of the subsystems. For this reason,a difference is observed at low frequencies. If the isotropic shell is assumed to be steel shell, then $f_r = 432.9$ and $f_c = 3991.5$. These estimated values are depicted in Figure 5. It can be observed that they are accurately estimated.

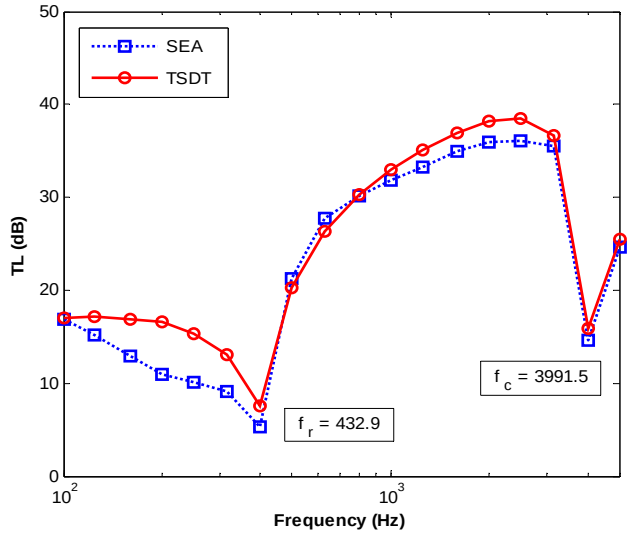

Figure 5: Comparison TL_{ave} for random incident angles of present study (TSDT) with SEA

In Figure 6 the results of present study compared with those of Koval's (1979) for a Graphite/Epoxy shell with the same condition as listed in Table 1. As it is demonstrated in the figure, some discrepancies are observed. It is happened as a result of using Flugge shell theory as well as applying only a transverse direction, in Koval's study.

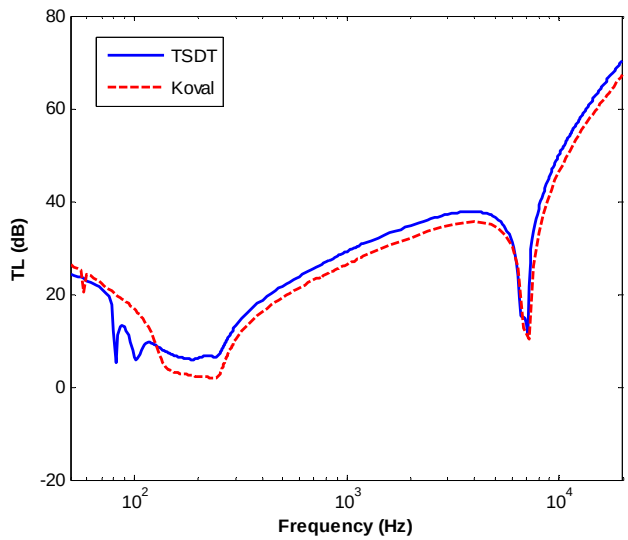

Figure 6: Comparison of present study (TSDT) with Koval

The present model is also compared with CST and FSDT used by Daneshjou et al. (2009) for a cylindrical shell made of Graphite/Epoxy. As depicted in Figures 7 to 9, the results show the present approach to be a much more accurate model because of using the TSDT and ignoring all previous simplifying assumptions by expanding the displacements as cubic functions of the thickness coordinate.

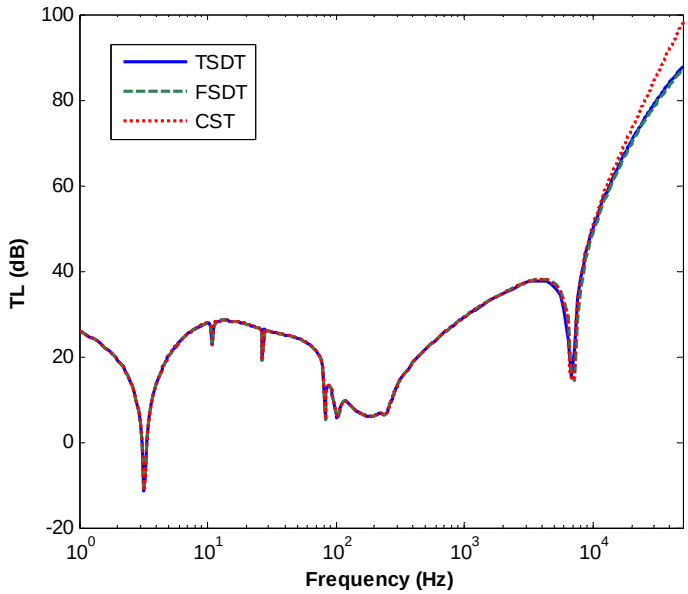

Figure 7: Comparison of present study (TSDT) with CST and FSDT for R/h=1000

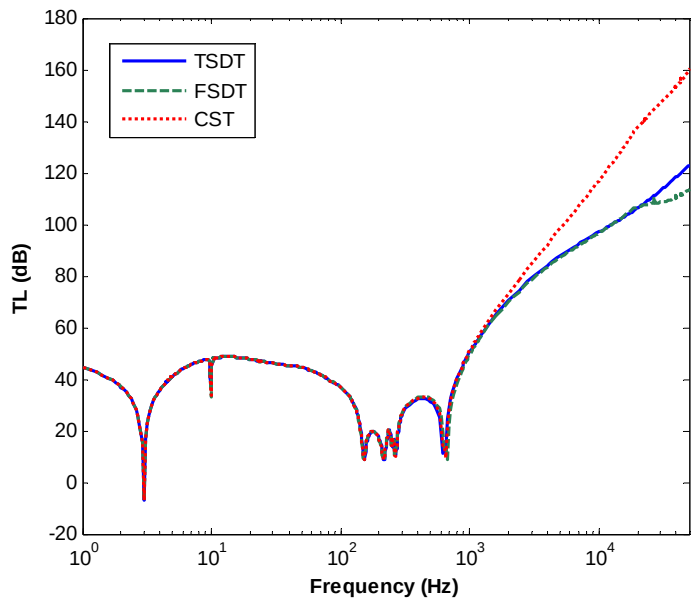

Figure 8: Comparison of present study (TSDT) with CST and FSDT for R/h=100

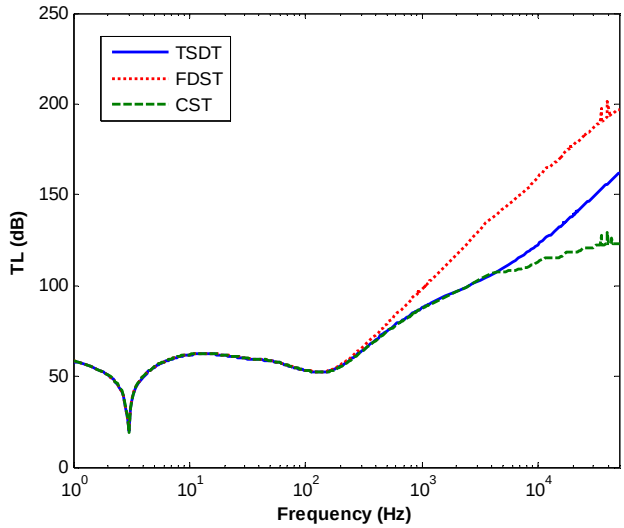

Figure 9: Comparison of present study (TSDT) with CST and FSDT for R/h=20

The results also indicate that TSDT are exactly similar with those of CST and FSDT in low frequencies. However, considerable errors are observed comparing the results of these theories at the high-frequency range, due to the effects of shear and rotation on TL. As depicted in Figures 8 and 9, with decrease of the ratio of R/h, the difference between TSDT and FSDT, is increased especially at high frequencies. It appears that, the effects of shear deformation on sound transmission are increased when the wave lengths are short enough, i.e., of the same order or less than the thickness of the shell. Table 3 provides a comparison between the computed results from TSDT, CST and FSDT with the different R/h ratios. The errors of these theories are presented in Table 4 in comparison with TSDT. Overall, according to the results shown in Table 3, for thick shells, there are some discrepancies between TSDT and FSDT in high frequencies (about 24% difference for $R/h = 20$) which is due to the less precise model of FSDT.

			Frequency (Hz)						
			100	1000	10000	20000	30000	40000	50000
TL (dB)	R/h=1000	CST	6.47	29.21	50.53	73.14	84.37	92.14	98.12
		FSDT	6.47	29.21	48.85	69.76	78.44	83.58	87.09
		TSDT	6.46	29.19	49.99	70.42	79.05	84.17	87.67
	R/h=100	CST	36.97	50.99	116.96	137.54	146.73	153.47	160.06
		FSDT	36.97	49.38	96.55	106.74	108.46	110.23	113.36
		TSDT	36.94	50.42	97.02	106.37	112.89	118.24	122.82
	R/h=20	CST	53.46	98.17	159.67	177.05	186.47	193.05	196.89
		FSDT	53.39	87.17	113.06	118.49	120.98	122.99	123.02
		TSDT	53.30	87.56	122.65	138.69	148.81	156.15	161.89

Table 3: Comparison between present study (TSDT) and FSDT for different frequencies and R/h.

			Frequency (Hz)						
			100	1000	10000	20000	30000	40000	50000
Error (%)	R/h=1000	CST	0.18	0.06	1.09	3.86	6.74	9.47	11.92
		FSDT	0.14	0.06	-2.28	-0.93	-0.77	-0.70	-0.67
	R/h=100	CST	0.09	1.11	20.55	29.30	29.98	29.80	30.32
		FSDT	0.08	-2.07	-0.49	0.34	-3.92	-6.77	-7.70
	R/h=20	CST	0.30	12.11	30.19	27.66	25.30	23.63	21.62
		FSDT	0.17	-0.45	-7.82	-14.57	-18.71	-21.23	-24.01

Table 4: Error (%) in comparison to present study (TSDT) for different frequencies and R/h.

Figures 7 to 9 and Table 3 indicate that with increasing the thickness, TL is enhanced and coincidence frequency shifts backward. At high frequencies, the wave lengths are very short in comparison to radius of the shell. Therefore, the radius of the shell does not influence the TL. Moreover, the results for CST are more than those of FSDT and TSDT at high frequencies. It is due to the fact that the shear and rotation are both significant in sound power transmission in high frequency range whereas the CST is completely ignored them. Also, the results presented in a forementioned figures and tables indicate that the difference between the results of TSDT and FSDT will become more significant in high frequencies especially for thick shells. Therefore, the need to use higher order shear deformation theory such as TSDT would increase. However, the FSDT seems to be a conservative criterion in comparison with TSDT in high frequencies as a result of demonstrating the least amounts of TL.

6 INVESTIGATIONS OF PARAMETERS

Figure 10 shows the effects of radius with R=0.5, 1.0 and 1.5 on TL. With increasing the shell radius, the TL is decreased in the stiffness-control region and the ring frequency shifts backward which are due to the curvature effect of the shell on its stiffness.

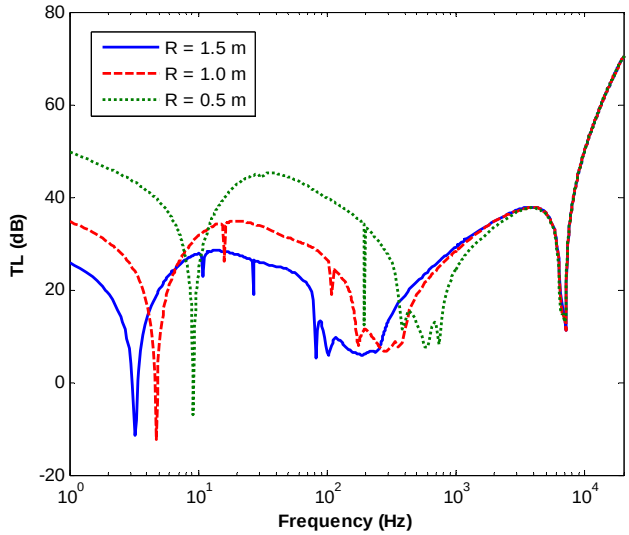

Figure 10: Investigation of R effect on TL curves

To investigate the effects of shell thickness, a comparison is made for three different shell thicknesses of $h = 1.5$, 1.0 and 0.5 mm in Figure 11. As it is clear, with increasing the thickness, TL is enhanced and coincidence frequency shifts backward.

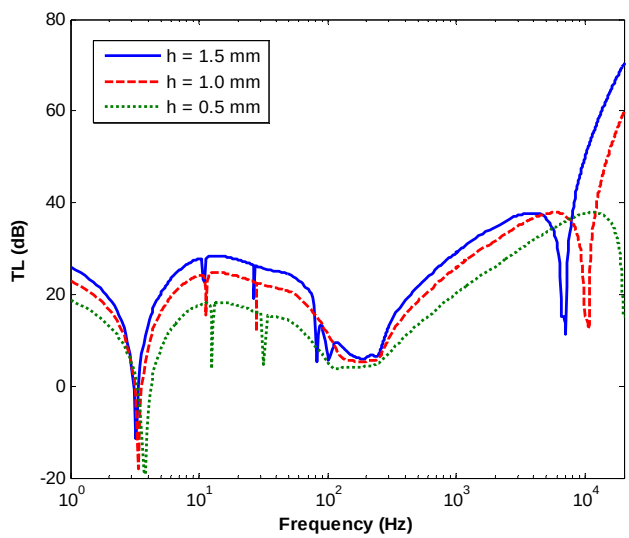

Figure 11: Investigation of h effect on TL curves

The results of present study for three different incident angles are shown in Figure 12. The inspection of this figure represents that increasing of α , leads to impressive descend of TL in the stiffness-controlled region whereas it is enhanced in the mass-controlled region. Also, with increasing the incident angle, the coincidence frequency shifts forward. This is due to the fact that increasing the incident angle leads to reduction of the radial wave number and growth of the axial wave number for the cylindrical shell.

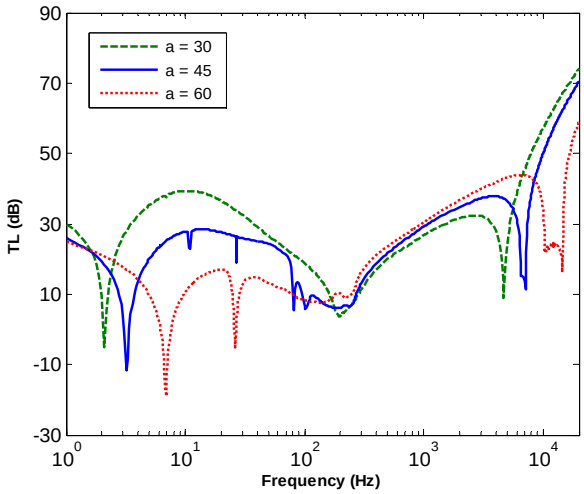

Figure 12: Investigation of α effect on TL curves

Figure 13 shows the effect of varying density on TL. The results indicate a direct relationship between density of the material and TL in the mass-controlled region. On the other hand, decreasing this parameter leads to forward shift of the ring frequency and backward shift of the coincidence frequency.

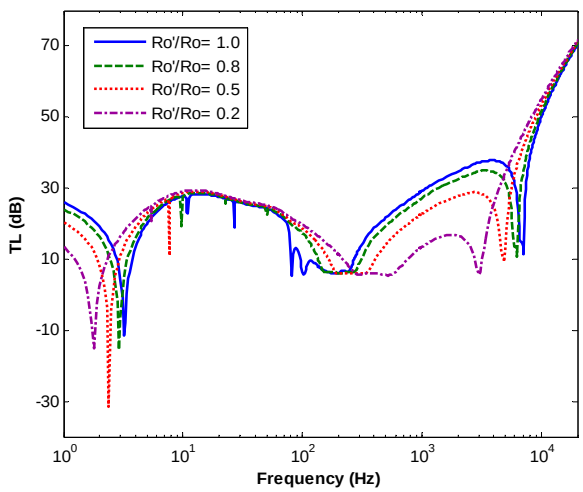

Figure 13: Investigation of ρ effect on TL curves

Figure 14 shows the effect of the different orthotropic material on TL. Materials chosen for the purpose of comparison are Graphite/Epoxy, Glass/Epoxy and Boron/Epoxy with the properties listed in Table 1. The figure shows that the material must be chosen properly to elevate TL at stiffness-controlled region. The results display that the Glass/Epoxy is the most effective in the mass controlled region because its density is the largest. As shown in Figure 14, the Boron/Epoxy, which has the highest stiffness, is the most effective one at the low frequency ranges. This could be anticipated as it is controlled with the stiffness below the ring frequency.

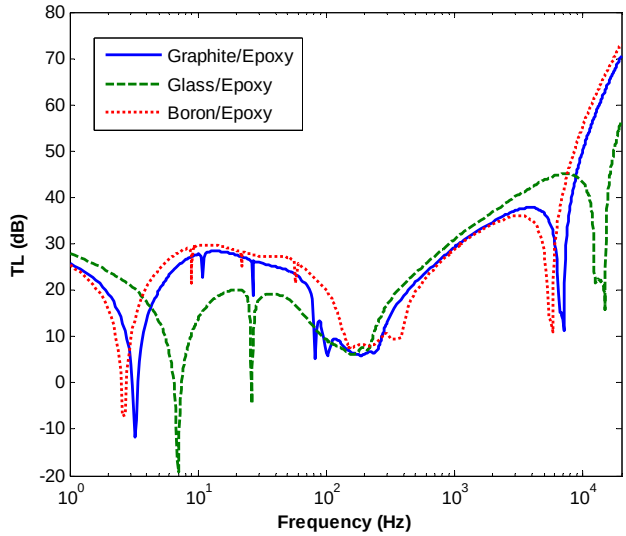

Figure 14: Investigation of different materials effect on TL curves

Finally, the influence of varying the mechanical properties of materials on the transmission loss of orthotropic cylindrical shell are studied and discussed. Figure 15 and 16 depict the effects of varying the Young's modulus on TL in η_1 and η_2 directions, respectively. A cylindrical shell made up of the Graphite/Epoxy is considered as the basis in this study. The different values of E'_{11} / E_{11} ratios are set to 1, 2, 5 and 10. The TL for the Graphite/Epoxy shell ($E'_{11} / E_{11} = 1$) is also illustrated. It can be seen from Figure 15 that increasing the stiffness in the η_1 - direction of an orthotropic shell increases the TL at low and high frequency bands. Also, the ring frequency remains unchanged in this case.

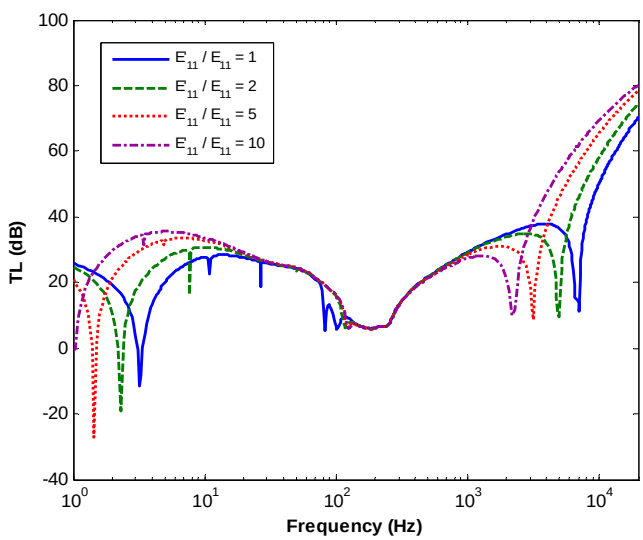

Figure 15: Investigation of E_{11} effect on TL curves

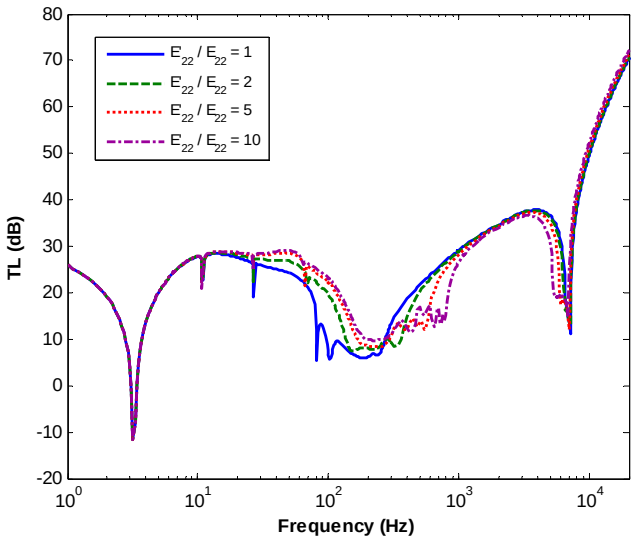

Figure 16: Investigation of E_{22} effect on TL curves

In addition, Figure 16 shows that the TL is enhanced around the ring frequency as a result of increasing the stiffness in the η_2 - direction. It is noted that the coincidence frequency is not sensitive to variation of this parameter.

Figure 17 shows the effect of decreasing G_{13} from $G'_{13} / G_{13} = 1$ to $G'_{13} / G_{13} = 0.1$ while the other mechanical properties of the cylindrical shell are kept constant. The wave numbers rise for small values of G_{13}, which will easily lead to loss of acoustic energy. Consequently, the transmission loss of orthotropic shell with small G'_{13} / G_{13} is lower than that with large G'_{13} / G_{13} in highfrequencies.

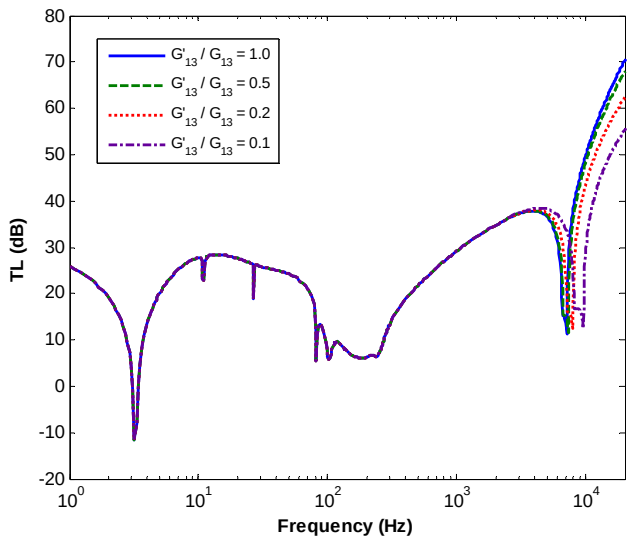

Figure 17: Investigation of G_{13} effect on TL curves

Figure 18 illustrates the variation of TL with reducing the shear modulus G_{23}. In this case, $G'_{23} / G_{23} = 1$, 0.5, 0.2 and 0.1 are chosen while the other properties remain constant. The results indicate that increasing the shear stiffness, G_{23}, will enhance the TL in orthotropic cylindrical shells at low frequencies. As can be seen from the Figure 17 and 18, the sound transmission loss might be enhanced by increasing the shear stiffnesses, G_{13} and G_{23}, only at high and low frequencies, respectively.

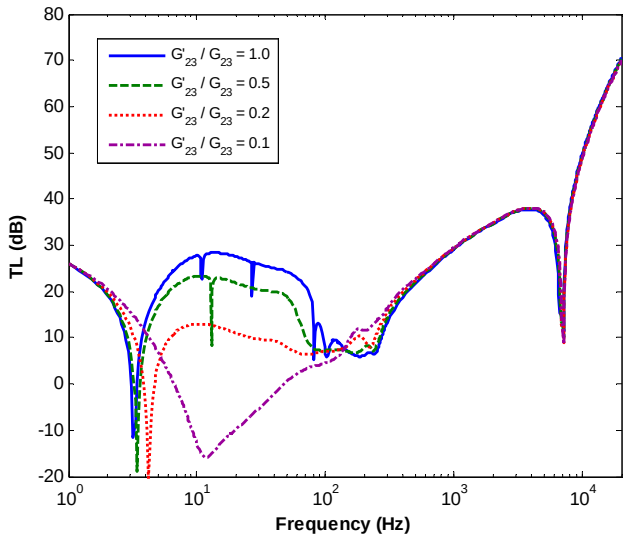

Figure 18: Investigation of G_{23} effect on TL curves

As shown in Figure 19, altering the shear stiffness G_{12} does not change the sound transmission loss.

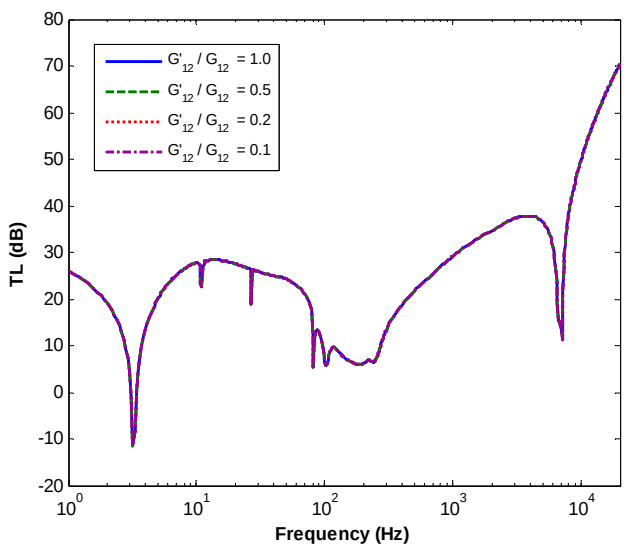

Figure 19: Investigation of G_{12} effect on TL curves

The effect of variation of Poisson's ratio (υ_{12}) on TL isdepicted in Figure 20. The value of υ_{12} is set to 0.4, 0.3, 0.2 and 0.1. However, Young's modulus and shear modulus are not changed.

As it is obvious, variation of Poisson's ratio has no significant effect on TL over the entire range of frequency.

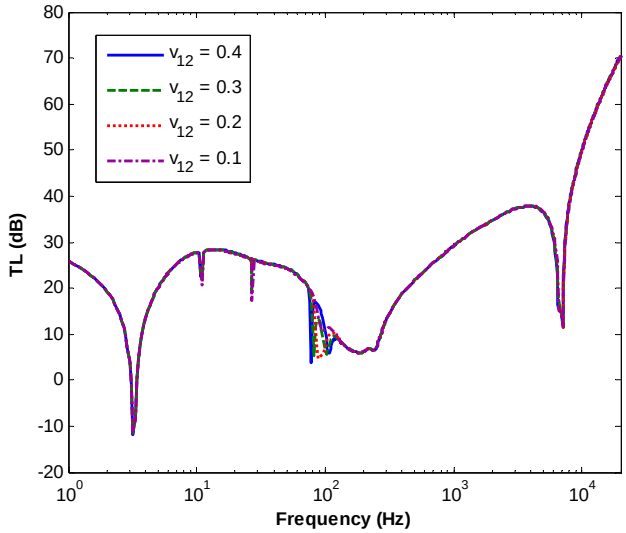

Figure 20: Investigation of υ_{12} effect on TL curves

The results discussed above, could be applied in designing the insulating structural shell. In other word, in such conditions that conducting experiments are rather difficult for measuring TL of the cylindrical shells, the proposed method would be useful to analyze such cases. This is the other contribution of this study to analyze the sound insulating properties. These results are hopefully practical for analyzing the sound insulating capabilities of a cylindrical shell.

7 CONCLUSIONS

An analytical model is developed in this paper for sound transmission across a thick-walled orthotropic cylindrical shell, based on the third-order shear deformation theory (TSDT). The cylindrical shell is assumed to be infinitely long and is subjected to an oblique plane sound wave with uniform airflow in the external fluid medium. Particularly, the following conclusions can be made:

1) For a thin-walled cylindrical shell, the TLs predicted using TSDT is of high compatibility with those of CST and FSDT in low frequencies. However, in high frequencies, the CST does not consider the effect of shear and rotation; therefore, it could not reach in agreements with other higher theories. In these frequencies the results from FSDT and TSDT are still in a good agreement which means that for the thin shells, there is no need to use more complicated theories such as TSDT.
2) For a thick-walled cylindrical shell, the difference between the results of TSDT and FSDT will become more significant except for low frequencies where shear and rotation effects

could be ignored. Therefore, the need to use higher order shear deformation theory such as TSDT would increase.

3) Since FSDT theory predicts lower amounts of TL in comparison with the other two methods, it could be used as the most conservative theory in sound insulator design. Nevertheless, TSDT would be the appropriate where the designers need perfect model.
4) Decreasing E_{11} tends to reduce TL of the cylinder in stiffness-controlled and coincidence controlled regions, where the coincidence frequency shifts upwards. It suggests that the TL might be enhanced by making the cylindrical shell stiffer in the axial direction than the circumferential direction.
5) TL of the cylindrical shell might be enhanced by increasing the E_{22} around the ring frequency. Moreover, it does not influence the coincidence frequency at all.
6) Increasing the shear stiffness G_{13} and G_{23} of orthotropic cylindrical shell might enhance the sound transmission loss only at high and low frequencies, respectively.
7) The results demonstrate that variation of the shear stiffness, G_{12}, and Poisson's ratio, υ_{12}, does not have a considerable effect on TL of cylindrical shells.

The proposed method can reasonably simulate the real phenomenon of sound transmission loss across orthotropic shells. Further work is under development to extend present analytical model for the prediction of sound transmission through a stiffened thick-walled laminated composite cylindrical shells.

APPENDIX

The elements of $\left[A\right]$ and $\left[B\right]$ matrices are given below:

$$A_{11} = -(-\bar{K}R\omega^2 + R^2{K_{1z}}^2 A_{11} + \frac{n^2}{R}A''_{66})$$

$$A_{12} = -(\frac{nK_{1z}}{R}\left(RA_{12} + RA_{66} + C_1\left(E_{12} + E_{66}\right)\right))$$

$$A_{13} = -\frac{K_{1z}}{R}(RA_{12} + C_1(-R^2\omega^2 K_4 + R^2{K_{1z}}^2 E_{11}) + n^2(E_{12} + E_{66} + E''_{66}))$$

$$A_{14} = \frac{1}{R}(\bar{J}R\omega^2 - n^2 B''_{66} + R^2{K_{1z}}^2\left(-B_{11} + C_1 E_{11}\right) + n^2 C_1 E''_{66})$$

$$A_{15} = -nK_{1z}(B_{12} + B_{66} - C_1(E_{12} + E_{66}))$$

$$A_{21} = -\frac{nK_{1z}}{R}\left(RA_{21} + RA_{66} + C_1\left(E_{21} + E_{66}\right)\right)$$

$$A_{22} = -\frac{1}{R^3}(-R^3\omega^2\bar{W} + n^2R^2A_{22} + R^2A_{44} + R^4{K_{1z}}^2 A'_{66} - 6R^2C_1D_{44} + 2n^2RC_1E_{22} -$$

$$4RC_1E_{44} + 2R^3C_1{K_{1z}}^2E'_{66} + 9R^2C_1^2F_{44} + 12RC_1^2G_{44} + n^2C_1^2H_{22} + 4C_1^2H_{44} + R^2C_1^2{K_{1z}}^2H'_{66})$$

$$A_{23} = -\frac{n}{R^3}(R^2\left(A_{22} + A_{44}\right) + RC_1(-R^2\omega^2W_4 - 6RD_{44} + R^2{K_{1z}}^2E_{21} + E_{22} + n^2E_{22} - 4E_{44} + R^2{K_{1z}}^2E_{66} + R^2{K_{1z}}^2E'_{66}) + C_1^2(9R^2F_{44} + 12RG_{44} + R^2{K_{1z}}^2H_{21} + n^2H_{22} + 4H_{44} + R^2{K_{1z}}^2H_{66} + R^2{K_{1z}}^2H'_{66}))$$

$$A_{24} = -\frac{nK_{1z}}{R}\left(RB_{12} + RB_{66} + C_1\left(RE_{21} + RE_{66} - F_{21} - F_{66} + C_1H_{21} + C_1H_{66}\right)\right)$$

$$A_{25} = \frac{1}{R^2}(\bar{G}R^2\omega^2 + R^2A_{44} - n^2RB_{22} - R^3{K_{1z}}^2B'_{66} - 6R^2C_1D_{44} + n^2RC_1E_{22} - 4RC_1E_{44} + R^3C_1{K_{1z}}^2E'_{66} - n^2C_1F_{22} + 9R^2C_1^2F_{44} - R^2C_1{K_{1z}}^2F'_{66} + 12RC_1^2G_{44} + n^2C_1H_{22} + 4C_1^2H_{44} + R^2C_1^2{K_{1z}}^2H'_{66})$$

$$A_{31} = -\frac{K_{1z}}{R}(RA_{21} + C_1(-R^2\omega^2K_4 + R^2{K_{1z}}^2E_{11} + n^2(E_{21} + E_{66} + E''_{66})))$$

$$A_{32} = -\frac{n}{R^3}(R^2\left(A_{22} + A_{44}\right) + RC_1(-R^2\omega^2W_4 - 6RD_{44} + R^2{K_{1z}}^2E_{21} + E_{22} + n^2E_{22} - 4E_{44} + R^2{K_{1z}}^2E_{66} + R^2{K_{1z}}^2E'_{66}) + C_1^2(9R^2F_{44} + 12RG_{44} + R^2{K_{1z}}^2H_{21} + n^2H_{22} + 4H_{44} + R^2{K_{1z}}^2H_{66} + R^2{K_{1z}}^2H'_{66}))$$

$$A_{33} = \frac{1}{R^3}(R^4\omega^2I_1 - R^2\left(A_{22} + n^2A_{44} + R^2{K_{1z}}^2A_{55}\right) + RC_1(6n^2RD_{44} + R^2{K_{1z}}^2(6RD_{55} - E_{12} - E_{21}) - 2n^2\left(E_{22} - 2E_{44}\right)) - C_1^2(-R^2\omega^2I_7\left(n^2 + R^2{K_{1z}}^2\right) + 9n^2R^2F_{44} + 9R^4{K_{1z}}^2F_{55} + 12n^2RG_{44} + R^4{K_{1z}}^4H_{11} + n^2R^2{K_{1z}}^2H_{12} + n^2R^2{K_{1z}}^2H_{21} + n^4H_{22} + 4n^2H_{44} + n^2R^2{K_{1z}}^2(2H_{66} + H'_{66} + H''_{66})))$$

$$A_{34} = \frac{K_{1z}}{R}(R\left(RA_{55} - B_{21}\right) + C_1(R^2\omega^2J_5 - 6R^2D_{55} + RE_{21} - R^2{K_{1z}}^2F_{11} - n^2F_{21} - n^2F_{66} - n^2F''_{66} + C_1^2(9R^2F_{55} + R^2{K_{1z}}^2H_{11} + n^2(H_{21} + H_{66} + H''_{66}))))$$

$$A_{35} = \frac{n}{R^2}(R\left(RA_{44} - B_{22}\right) + C_1(R^2\omega^2J_5 - 6R^2D_{44} + RE_{22} - 4RE_{44} - n^2F_{22} - R^2{K_{1z}}^2(F_{12} + F_{66} + F'_{66}) + C_1^2(9R^2F_{44} + 12RG_{44} + R^2{K_{1z}}^2(H_{12} + H_{66} + H'_{66}) + n^2H_{22} + 4H_{44})))$$

$$A_{36} = H_n^2(K_{1r}R_i)$$

$$A_{37} = -H_n^1(K_{3r}R_i)$$

$$A_{41} = \frac{1}{R}\Big(\tilde{K}R\omega^2 - n^2 B''_{66} + R^2 {K_{1z}}^2 \big(-B_{11} + C_1 E_{11}\big) + n^2 C_1 E''_{66} \Big)$$

$$A_{42} = -\frac{nK_{1z}}{R}\Big(RB_{12} + RB_{66} + C_1\big(RE_{12} + RE_{66} - F_{12} - F_{66} + C_1 H_{12} + C_1 H_{66}\big)\Big)$$

$$A_{43} = \frac{K_{1z}}{R}(R\big(RA_{55} - B_{12}\big) + C_1(R^2\omega^2 J_5 - 6R^2 D_{55} + RE_{12} - R^2 {K_{1z}}^2 F_{11} - n^2 F_{12} -$$
$$n^2 F_{66} - n^2 F''_{66} + C_1^2(9R^2 F_{55} + R^2 {K_{1z}}^2 H_{11} + n^2(H_{12} + H_{66} + H''_{66}))))$$

$$A_{44} = -\frac{1}{R}(-\tilde{J}R\omega^2 + R^2 A_{55} - 6R^2 C_1 D_{55} + n^2 D''_{66} + 9R^2 C_1^2 F_{55} - 2n^2 C_1 F''_{66} +$$
$$R^2 {K_{1z}}^2\big(D_{11} - 2C_1 F_{11} + C_1^2 H_{11}\big) + n^2 C_1^2 H''_{66})$$

$$A_{45} = -nK_{1z}(D_{12} + D_{66} + C_1(-2F_{12} - 2F_{66} + C_1(H_{12} + H_{66})))$$

$$A_{51} = -nK_{1z}(B_{21} + B_{66} - C_1(E_{21} + E_{66}))$$

$$A_{52} = \frac{1}{R^2}(R^2\omega^2\tilde{W} + R^2 A_{44} - n^2 RB_{22} - R^3 {K_{1z}}^2 B'_{66} - 6R^2 C_1 D_{44} + n^2 RC_1 E_{22} -$$
$$4RC_1 E_{44} + R^3 C_1 {K_{1z}}^2 E'_{66} - n^2 C_1 F_{22} + 9R^2 C_1^2 F_{44} - R^2 C_1 {K_{1z}}^2 F'_{66} + 12RC_1^2 G_{44} +$$
$$n^2 C_1^2 H_{22} + 4C_1^2 H_{44} + R^2 C_1^2 {K_{1z}}^2 H'_{66})$$

$$A_{53} = \frac{n}{R^2}(R\big(RA_{44} - B_{22}\big) + C_1(R^2\omega^2 J_5 - 6R^2 D_{44} + RE_{22} - 4RE_{44} - n^2 F_{22} -$$
$$R^2 {K_{1z}}^2(F_{21} + F_{66} + F'_{66}) + C_1^2(9R^2 F_{44} + 12RG_{44} + R^2 {K_{1z}}^2(H_{21} + H_{66} + H'_{66}) +$$
$$H_{22} + 4H_{44})))$$

$$A_{54} = -nK_{1z}(D_{21} + D_{66} + C_1(-2F_{21} - 2F_{66} + C_1(H_{21} + H_{66})))$$

$$A_{55} = -\frac{1}{R}(-\tilde{J}R\omega^2 + R^2 A_{44} + n^2 D_{22} - 6R^2 C_1 D_{44} + R^2 {K_{1z}}^2 D'_{66} - 4RC_1 E_{44} - 2n^2 C_1 F_{22} +$$
$$9R^2 C_1^2 F_{44} - 2R^2 C_1 {K_{1z}}^2 F'_{66} + 12RC_1^2 G_{44} + n^2 C_1^2 H_{22} + 4C_1^2 H_{44} + R^2 C_1^2 {K_{1z}}^2 H'_{66})$$

$$A_{63} = -\Big(\rho_1\omega^2 + \rho_1 V^2 {K_{1z}}^2 + 2\rho_1 V\omega K_{1z}\Big)$$

$$A_{66} = H'^2_n(K_{1r}R_i)K_{1r}$$

$$A_{73} = -\rho_3\omega^2$$

$$A_{77} = H'^1_n(K_{3r}R_i)K_{3r}$$

$$B_3 = -\epsilon_n\big(j\big)^n J_n(K_{1r}R_i)P_0$$

$$B_6 = -P_0\epsilon_n\big(j\big)^n J'_n(K_{1r}R_i)K_{1r}$$

References

Smith, J. P. W., (1957). Sound Transmission Through Thin Cylindrical Shells. Journal of the Acoustical Society of America 29:721-729.

White, P. H., (1966). Sound Transmission Through a Finite, Closed, Cylindrical Shell. Journal of the Acoustical Society of America 40:1124-1130.

Koval, L. R., (1976). Sound Transmission into a Thin Cylindrical Shell under "Flight Conditions ". Journal of Sound and Vibration 48:265-275.

Koval, L. R., (1979). Sound Transmission into an Orthotropic Shell. Journal of Sound and Vibration 63:51-59.

Nelson, H. C., Zapatowski B., Bernstein M., (1958).Vibration Analysis of Orthogonally Stiffened Circular Fuselage and Comparison with Experiment. Proceedings of the Institute of Aeronautical Sciences National Specialist's Meeting on Dynamics and Aeroelasticity, pp. 77–87.

Koval,L.R., (1980). Sound Transmission into a Laminated Composite Cylindrical Shell. Journal of Sound and Vibration 71:523-530.

Blaise, A., Lesueur, C., Gotteland, M. and Barbe M., (1991). Sound Transmission into an Orthotropic Infinite Shell: Comparison with Koval's Results and Understanding of Phenomena. Journal of Sound and Vibration 150:233-243.

Blaise, A., Lesueur, C., (1992). Acoustic Transmission Through a 2-D Orthotropic Multi-layered Infinite Cylindrical Shell. Journal of Sound and Vibration 155:95-109.

Blaise, A., Lesueur, C., (1994). Acoustic Transmission Through a "3-D" Orthotropic Multi-Layered Infinite Cylindrical Shell, Part I: Formulation of the Problem. Journal of Sound and Vibration 171:651-664.

Blaise, A., Lesueur, C., (1994). Acoustic Transmission Through a "3-D" Orthotropic Multi-Layered Infinite Cylindrical Shell, Part II: Validation and Numerical Exploitation for Large Structures. Journal of Sound and Vibration 171:665-680.

Tang, Y. Y., Silcox, R. J. and Robinson, J. H., (1996). Sound Transmission Through a Cylindrical Sandwich Shell with Honeycomb Core. Proceedings of the 34th AIAA aerospace science meeting and exhibit. (USA).

Lee, J. H., Kim, J., (2002). Analysis and Measurement of Sound Transmission Through a Double-Walled Cylindrical Shell. Journal of Sound and Vibration 251:631-649.

Lee, J. H., Kim, J., (2003). Study on Sound Transmission Characteristics of a Cylindrical Shell using Analytical and Experimental Models. Journal of Applied Acoustics 64:611-632.

Ghinet, S., Atalla, N. and Osman, H., (2006). Diffuse Field Transmission into Infinite Sandwich Composite and Laminate Composite Cylinders. Journal of Sound and Vibration 289:745-778.

Daneshjou, K., Nouri, A. and Talebitooti, R., (2007). Sound Transmission Through Laminated Composite Cylindrical Shells using Analytical Model, Arch Applied Mechanics 77:363-379.

Daneshjou, K., Nouri, A. and Talebitooti, R., (2008). Analytical Model of Sound Transmission Through Laminated Composite Cylindrical Shells Considering Transverse Shear Deformation. Appl. Math. Mech. Engl. Ed. 29:1165-1177.

Daneshjou, K., Nouri, A. and Talebitooti R., (2009). Analytical Model of Sound Transmission Through Orthotropic Cylindrical Shells with Subsonic External Flow. Journal of Aerospace Science and Technology 13:18-26.

Daneshjou, K., Shokrieh, M.M., Ghorbani Moghaddam, M., Talebitooti, R., (2010). Analytical Model of Sound Transmission through Relatively Thick FGM Cylindrical Shells Considering Third Order Shear Deformation Theory, Composite Structure 93: 67-78.

Reddy, J. N. (2003). Mechanics of Laminated Composite Plates and Shells: Theory and Analysis, Second Edition, CRC Press.

Qatu, M. S. (2004). Vibration of Laminated Shells and Plates, Elsevier Academic Press.

Chakrabarti, A., Kumar, A. and Ketkar, M., (2013). Analysis of Laminated Composite Skew Shells using Higher Order Shear Deformation Theory. Latin American Journal of Solids and Structures 10:891-919.

Lee, S. J., Reddy, J. N., (2004). Vibration Suppression of Laminated Shell Structures Investigated using Higher Order Shear Deformation Theory. Journal of Smart Mater. Struct. 13:1176–1194.

Howe, M. S. (2000). Acoustics of Fluid Structure Interactions, Cambridge University Press.

Pierce, A. D. (1981). Acoustics, McGraw-Hill Press.

Yuan, C., Bergsma, O. and Beukers, A., (2012). Sound Transmission Loss Prediction of the Composite Fuselage with Different Methods.Journal of Appl Compos Mater. 19:883-865.